

NLO QCD corrections to WZ +jet production with leptonic decays

Francisco Campanario

*Institute for Theoretical Physics, Karlsruhe Institute of Technology,
76128 Karlsruhe, Germany*

Christoph Englert

*Institute for Theoretical Physics, Karlsruhe Institute of Technology,
76128 Karlsruhe, Germany
and
Institute for Theoretical Physics, Heidelberg University,
69120 Heidelberg, Germany*

Stefan Kallweit

*Paul Scherrer Institute, Würenlingen and Villigen
5232 Villigen PSI, Switzerland*

Michael Spannowsky

*Institute of Theoretical Science, University of Oregon,
Eugene, OR 97403-5203, USA*

Dieter Zeppenfeld

*Institute for Theoretical Physics, Karlsruhe Institute of Technology,
76128 Karlsruhe, Germany*

ABSTRACT: We compute the next-to-leading order QCD corrections to WZ +jet production at the Tevatron and the LHC, including decays of the electroweak bosons to light leptons with all off-shell effects taken into account. The corrections are sizable and have significant impact on the differential distributions.

KEYWORDS: QCD, NLO Computations, Jets.

Contents

1. Introduction	1
2. Details of the calculation	2
3. Numerical results	4
3.1 Event selection	5
3.2 Production cross sections at the Tevatron	6
3.3 Production cross sections at the LHC	7
3.4 Differential distributions at the LHC	9
4. Summary	11

1. Introduction

At the Large Hadron Collider (LHC) as well as at the Tevatron, electroweak di-boson production in association with a hard jet represents an important class of processes, of either signal or background character in various searches for Standard Model (SM) and beyond. The rates are large, especially at the LHC by accessing the gluon density at small momentum fraction, and next-to-leading order (NLO) QCD corrections have turned out sizable in a series of recent publications [1–5] providing WW+jet, ZZ+jet, and $W^\pm\gamma$ +jet production at NLO QCD precision at hadron colliders. In this paper, we supplement NLO QCD precision to

$$p\bar{p}, pp \rightarrow 3 \text{ leptons} + \cancel{E}_T + \text{jet} + X,$$

i.e. to $W^\pm Z$ +jet production including full leptonic decays. We give cross sections for LHC and Tevatron collisions and also discuss the corrections' phase-space dependence by investigating differential correction factors at the LHC.

To verify our results, special care is devoted to independent numerically stable implementations of the processes, yielding two independent fully-flexible Monte Carlo programs, based on different approaches.

We organize this work in the following way: In section 2 we provide an overview of the two programs we have employed for the numerical results of this paper, to which section 3 is devoted. We first focus on on-shell production at the Tevatron and the LHC in sections 3.2 and 3.3, respectively, and then move on to discuss the differential impact of the QCD corrections for the LHC setup in more phenomenological detail in section 3.4. Section 4 concludes with a summary of the work presented in this paper.

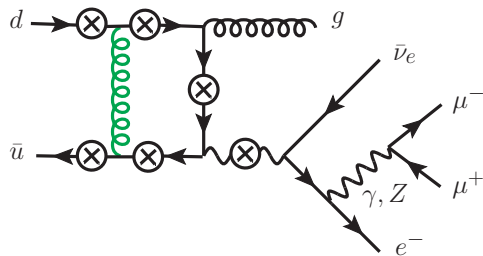


Figure 1: Representative Feynman graph contributing to $pp, pp \rightarrow \bar{\nu}_e e^- \mu^+ \mu^- + X$. The crosses mark points where the $\gamma, Z \rightarrow \mu^+ \mu^-$ decay topology can be inserted. Indicated is also the exchange of a virtual gluon, which gives rise to self-energy, triangle, box, and pentagon topologies. Not shown are topologies that result from closed fermion loops, non-abelian graphs, and real emission topologies. All other subprocesses can be recovered from the shown graph by flavour summation and/or crossing.

2. Details of the calculation

We invoke a dedicated system of checks and balances to validate our calculation. In particular, we have compared two different Monte Carlo implementations, relying on distinct approaches. The comparisons involve cross checks at the amplitude level for a fixed phase-space point as well as comparisons of integrated cross sections. In both cases we find agreement on the level of double-precision accuracy or agreement within the statistical errors, respectively, for different choices of renormalization and factorization scales and cuts.

Our independent calculations are based on the approaches of [2–4], where the used methods have already been described in detail. Hence, we limit ourselves to the bare necessities to make this paper self-consistent and refer the interested reader to the above publications for more details.

Program 1 We generalize the NLO QCD calculation of $W\gamma$ +jet production (including leptonic decays) [4] to WZ +jet production. The leading order (LO) matrix elements at $\mathcal{O}(\alpha^4 \alpha_s)$, cf. figure 1 are calculated with HELAS routines [6] generated with MADGRAPH [7]. Our phase-space implementation is based on routines readily present in the VBFNLO suite [8], which were already applied in the context of NLO QCD vector-boson-fusion WZ +2jets production, including leptonic decays, in various scenarios [9, 10]. Nonetheless integrated results for the different subprocesses have been checked against SHERPA [11], yielding agreement within statistical errors on per-mill level.

The virtual corrections are combined to groups that include all loop diagrams derived from a born-level configuration, i.e. all self-energy, triangle, box and pentagon corrections to a quark line with three attached gauge bosons, which are computed as effective decay currents in case of the electroweak bosons, are combined to a single numerical routine. This leaves a set of universal building blocks, which were already appropriately assembled to determine the one-loop contribution to $W\gamma$ +jet production (cf. [4] for details on the verification of the implementation against an independent approach). The generalization

to WZ+jet becomes trivial by replacing the photon polarization vector by the effective Z decay current multiplying the appropriate coupling. These building blocks are set up using in-house routines within the framework of FEYN CALC [12] and FEYNARTS [13]. They invoke the Passarino–Veltman reduction [14] up to boxes and the Denner–Dittmaier reduction [15] for pentagons. The remaining fermionic loop corrections are derived via algebraic calculations using FEYN CALC, which is subsequently processed to FORTRAN routines with in-house routines. The scalar integrals that are not already present in the VBFNLO framework are supplemented from the Ellis–Zanderighi library [16]. All effective decay currents are evaluated by means of HELAS routines generated with MADGRAPH, which are modified to fit our purpose of calculating the one-loop amplitude.

To speed up the numerical implementation of the numerous subprocesses that show up as part of the real emission, we computed the real emission matrix element using the spinor helicity formalism of [17]. We store intermediate numerical results common to all subprocesses and re-use them whenever possible. All matrix elements have been checked explicitly against code generated from MADGRAPH.

The infrared (IR) singularities are subtracted applying the dipole subtraction of [18], while the corresponding LO matrix elements and currents for the subtraction kinematics are computed using HELAS routines. We also apply necessary bookkeeping in order not to waste computing time. The IR poles of the virtual amplitude are cancelled against the real-emission ones algebraically, and we perform the integration of finite collinear terms as part of the real-emission integration by appropriately mapping the born-type configuration as done in [19].

The code will become publicly available with an upcoming update of VBFNLO.

Program 2 We proceed essentially in the same way as in the calculation of WW+jet, which is discussed in some detail in Refs. [2,3]. All LO helicity amplitudes are calculated by application of the Weyl–van-der-Waerden formalism (as described in Ref. [20]). In this approach, the implementation of the gauge-boson decays can be easily realized by replacing the polarization bispinors of the gauge bosons with expressions containing the currents of the decay leptons. Allowing for off-shell gauge bosons and still respecting gauge invariance requires the inclusion of diagrams which do not contain two simultaneously resonant gauge-boson propagators. However, all diagrams of this kind can be constructed from W+jet-production amplitudes by replacing the W-boson polarization bispinor with an appropriate expression describing its decay into 4 leptons. Additionally, diagrams with intermediate photons instead of Z bosons have to be taken into account. It is worth noting that the described replacements are exactly the same for the LO and for all components of the NLO QCD calculation—in other words, the bispinor replacements are universal. In particular, no new types of loop diagrams show up in the virtual corrections.

Again, the dipole subtraction formalism of [18] is applied to rearrange the IR divergences between real and virtual corrections at NLO QCD.

The loop diagrams and amplitudes are generated by FEYNARTS 3.4 [13] and then further manipulated with FORMCALC 6.0 [21] to automatically produce FORTRAN code. The whole reduction of tensor to scalar integrals is done with the help of the LOOPTOOLS

library [21], which also employs the Denner–Dittmaier method [15] for the 5-point tensor integrals, Passarino–Veltman [14] reduction for the lower-point tensors, and the FF package [22, 23] for the evaluation of regular scalar integrals. The IR (soft and collinear) singular 3- and 4-point integrals in dimensional regularization are linked to this library as in the WW+jet calculation. Again, the explicit results of Ref. [24] for the vertex and of Ref. [25] for the box integrals (with appropriate analytical continuations) are taken. Actually the FORMCALC package assumes a four-dimensional regularization scheme for IR divergences, i.e. rational terms of IR origin are neglected by FORMCALC. However, in Ref. [26] it was generally shown that such rational terms consistently cancel if UV and IR divergences are properly separated. Thus we could use the algebraic result of FORMCALC for the unrenormalized amplitudes without any modification, apart from supplementing the needed IR-singular scalar integrals.

To receive the real-correction matrix elements we also employ the Weyl–van-der-Waerden formalism. The dipoles needed to cancel the divergences in the respective subprocesses are automatically generated from the born-level helicity amplitudes. To achieve numerical stability on a high-accuracy level, the phase-space integration is performed by a multi-channel Monte Carlo integrator [27] with weight optimization [28], which has been written in C++ and checked in detail in the calculation of WW+jet. Additional channels basing on dipole kinematics are automatically included to improve the efficiency of the integration of the dipole-subtracted real-emission matrix elements. When the full calculation with off-shell gauge bosons is considered, only channels according to doubly-resonant diagrams are included, which turns out to provide already sufficient numerical stability.

Both numerical programs account for finite width effects of the electroweak gauge bosons (when considering their leptonic decays) with a fixed-width scheme, which is also the scheme used by MADGRAPH: while we calculate with Breit-Wigner propagators of the W and Z bosons we keep the weak mixing angle real. To justify this approach, which breaks gauge invariance, we compared the results to a calculation performed applying the complex-mass scheme [29] in one of the programs. We find an agreement on the per-mill level between the two calculations, so the effect of gauge-invariance breaking turns out to be sufficiently small to be ignored here.

3. Numerical results

Throughout, we use CTEQ6M parton distributions [30] at NLO, and the CTEQ6L1 set at LO. We choose $M_Z = 91.1876$ GeV, $M_W = 80.425$ GeV, and $G_F = 1.16637 \times 10^{-5}$ GeV⁻² as electroweak input parameters and derive the electromagnetic coupling α and the weak mixing angle $\sin \theta_w$ via SM tree-level relations. The LO and NLO running of α_s are determined by $\alpha_s^{\text{LO}}(M_Z) = 0.130$ and $\alpha_s^{\text{NLO}}(M_Z) = 0.118$ for five active flavors, respectively.

The center-of-mass energy is fixed to $\sqrt{s} = 14$ TeV for LHC and $\sqrt{s} = 1.96$ TeV for Tevatron collisions, respectively. We consider both on-shell production of the electroweak bosons and their decays to distinct species of light leptons, e. g. $W^- \rightarrow e^- \bar{\nu}_e$ and $Z \rightarrow \mu^- \mu^+$, treating these leptons as massless. The CKM matrix is taken to be diagonal,

and we neglect bottom contributions throughout because they are numerically negligible anyway and can even be further suppressed by b-tagging. To be more precise, we neglect the—finite and negligibly small—contribution from real correction minus subtraction terms if external bottom quarks are involved. In the fermionic quark loops and, correspondingly, the I -operator, we keep all six quark flavours. A non-diagonal CKM matrix decreases our LHC results only at the per-mill level because gluon-induced subprocesses dominate the cross section. In case of a Cabibbo-like block-diagonal CKM matrix, the contribution from this subset of subprocesses is not affected if all light quarks are summed over. The correction for the Tevatron cross section is about 3% due to the dominance of quark-induced subprocesses. These corrections are well below the residual scale dependence at NLO QCD. The final-state partons are recombined to massless jets via the algorithm of [31] with resolution parameter $R = 1.0$. Other jet algorithms, like the kT algorithm of Ref. [32] have also been implemented in program 1.

3.1 Event selection

To analyze the impact of the NLO QCD corrections on the total production cross sections at both the Tevatron and the LHC, we apply a rather inclusive set of cuts. In case of on-shell W and Z boson production, the jets are required to have a transverse momentum of

$$p_{T,\text{jet}} \geq 50 \text{ GeV} , \quad (3.1)$$

which is the only selection criterion we impose for the calculation of the cross sections of Secs. 3.2 and 3.3. In case of included leptonic decays of the electroweak bosons, we account for finite jet-detection coverage by requiring the jets to have rapidities

$$|\eta_j| \leq 4.5 \quad (3.2)$$

in addition to the cut on $p_{T,\text{jet}}$ of Eq. (3.1). However, with the used cut value for $p_{T,\text{jet}}$, the additional effect of this cut is completely negligible at the given collider energies. All leptons are required to lie in

$$|\eta_\ell| \leq 2.5 \quad (3.3)$$

with transverse momenta of

$$p_{T,\ell} \geq 25 \text{ GeV} . \quad (3.4)$$

The overall missing transverse momentum is chosen to be

$$\cancel{p}_T \geq 25 \text{ GeV} . \quad (3.5)$$

The leptons have to be separated in the azimuthal-angle–pseudorapidity plane by

$$R_{\ell\ell'} = (\Delta\phi_{\ell\ell'}^2 + \Delta\eta_{\ell\ell'}^2)^{1/2} \geq 0.2 , \quad (3.6)$$

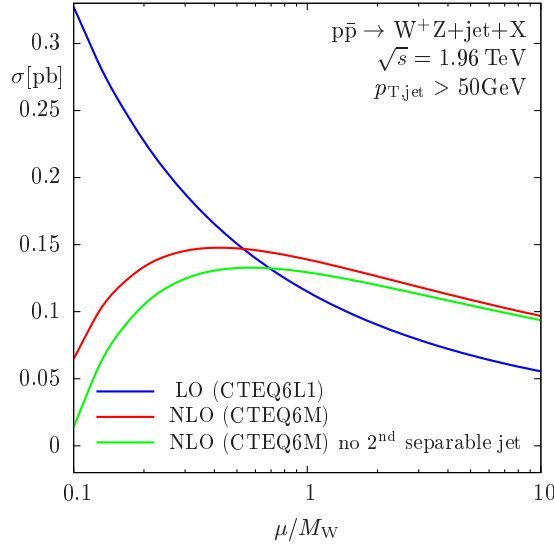


Figure 2: Fixed-scale variation of $\mu_R = \mu_F = \mu$ for on-shell $W^\pm Z + \text{jet}$ production at the Tevatron.

and for their separation from observable jets we choose

$$R_{\ell j} \geq 0.4. \quad (3.7)$$

It is customary from a theoretical point of view to study also the cross sections' behaviour with a veto applied to the second resolved jet in the context of mono-jet production: it was shown [1–5] that this additional veto yields highly stabilized NLO exclusive cross sections in the context of $WW + \text{jet}$, $ZZ + \text{jet}$, and $W\gamma + \text{jet}$ production. Indeed, given the similarities of the processes from a QCD point of view, identical properties for $WZ + \text{jet}$ production are evident. We will discuss the phenomenological problems of the additional jet veto in detail in section 3.4.

3.2 Production cross sections at the Tevatron

For on-shell $W^\pm Z + \text{jet}$ production from Tevatron collisions with the additional requirement of (3.1), we compute a total inclusive and exclusive $WZ + \text{jet}$ on-shell cross sections and K factors

$$K = \frac{\sigma^{\text{NLO}}}{\sigma^{\text{LO}}} \quad (3.8)$$

of

$$\sigma_{\text{incl}}^{\text{NLO}}(W^\pm Z + \text{jet}) = (139.01 \pm 0.10) \text{ fb} \quad [K = 1.209], \quad (3.9)$$

$$\sigma_{\text{excl}}^{\text{NLO}}(W^\pm Z + \text{jet}) = (129.40 \pm 0.10) \text{ fb} \quad [K = 1.125], \quad (3.10)$$

which are dominated by $q\bar{Q}$ induced processes due to the relatively large momentum fraction of the incoming partons $x \sim 0.2$ at LO, which we infer from the Monte Carlo simulation. The total correction of 21% with respect to LO at the central scale is sizable. Nonetheless,

including the leptonic decays decreases the cross sections to phenomenologically subdominant size, unless the transverse momentum requirement for jets is reduced substantially. We therefore limit ourselves to quoting total on-shell production rates at the Tevatron and focus on differential distributions at the LHC only.

A lower bound on the scale uncertainties of the cross sections can be inferred e. g. from varying the fixed renormalization and factorization scales by a factor of two around the central value $\mu_R = \mu_F = M_W$, cf. figure 2. Doing so, the LO approximation exhibits a scale variation of 31% which is decreased to 9% by including NLO-inclusive precision.

3.3 Production cross sections at the LHC

Turning to the more energetic LHC collisions, we find a completely different situation compared to the Tevatron. The proton is typically probed at much lower momentum fractions $x \sim 0.02$ at LO (as the Monte Carlo calculation shows), so that the qg -induced initial states dominate the total rate. The total NLO-inclusive cross sections are

$$\sigma_{\text{incl}}^{\text{NLO}}(\text{W}^- \text{Z} + \text{jet}) = (7.495 \pm 0.008) \text{ pb} \quad [K(\text{W}^- \text{Z} + \text{jet}) = 1.298] \quad , \quad (3.11)$$

$$\sigma_{\text{incl}}^{\text{NLO}}(\text{W}^+ \text{Z} + \text{jet}) = (12.061 \pm 0.013) \text{ pb} \quad [K(\text{W}^+ \text{Z} + \text{jet}) = 1.260] \quad , \quad (3.12)$$

for a scale choice $\mu_R = \mu_F = M_W$.

In close analogy to [1–5], the di-jet contribution re-introduces a substantial dependence on the renormalization scale μ_R via the dominating qg -induced channels. This becomes apparent by checking the variation for several scales intrinsic to the total cross section in figure 3.

The cross sections' qualitative scaling behaviour does not depend on the choice of the intrinsic scale, and the characteristic increase of the NLO-inclusive cross sections at small scales $\mu = \mu_R = \mu_F$ reflects the renormalization scale dependence of the di-jet contribution, which is a leading order- α_s contribution to our NLO computation.

This μ_R dependence of di-jet contributions can be effectively buffered by imposing an additional veto on events with two resolved jets, which gives rise to total NLO-exclusive rates for $\mu_R = \mu_F = M_W$ of

$$\sigma_{\text{excl}}^{\text{NLO}}(\text{W}^- \text{Z} + \text{jet}) = (4.981 \pm 0.009) \text{ pb} \quad [K(\text{W}^- \text{Z} + \text{jet}) = 0.862] \quad , \quad (3.13)$$

$$\sigma_{\text{excl}}^{\text{NLO}}(\text{W}^+ \text{Z} + \text{jet}) = (7.831 \pm 0.014) \text{ pb} \quad [K(\text{W}^+ \text{Z} + \text{jet}) = 0.818] \quad . \quad (3.14)$$

Varying again $\mu_R = \mu_F$ by a factor two around the central values in figure 3 amounts to scale uncertainties of 8% ($\text{W}^- \text{Z} + \text{jet}$) and 8% ($\text{W}^+ \text{Z} + \text{jet}$) of the total inclusive cross sections at the LHC. For the vetoed sample, the scale dependence is reduced to about 5% for $\text{W}^- \text{Z} + \text{jet}$, and 6% for $\text{W}^+ \text{Z} + \text{jet}$ production.

The improved perturbative stability of the exclusive cross sections should be interpreted with caution. While jet-vetoing is a straightforward exercise in the context of fixed-order Monte Carlo calculations, its phenomenological consequences are generally highly delicate, both from the theoretical and the experimental side. The small total correction along with the stability against variations of $\mu_R = \mu_F$ of the exclusive cross sections should therefore not be misinterpreted as a guideline to stable LHC predictions *per se*, but as a

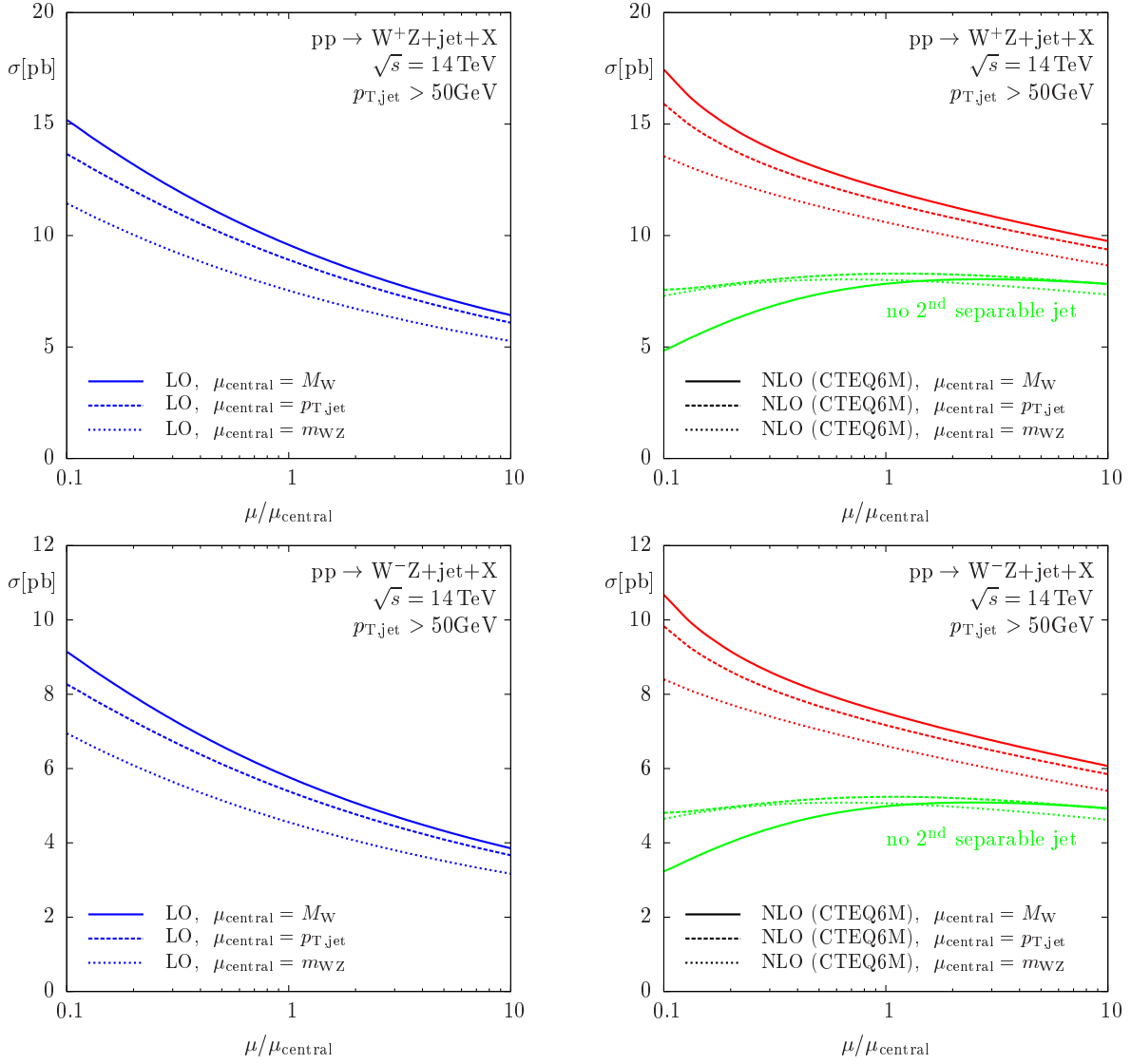


Figure 3: Scale variation for on-shell W^+Z +jet (upper plots) and W^-Z +jet (lower plots) production at the LHC. The identified renormalization and factorization scales $\mu_R = \mu_F = \mu$ are varied with respect to the fixed scale M_W , the maximum $p_{T,\text{jet}}$, and the invariant mass m_{WZ} . The plots on the left show cross sections at LO, those on the right at NLO QCD accuracy.

significant perturbative improvement of WZ +jet production up to the specified threshold value of $p_{T,\text{jet}}$. This is visible in the differential jet- p_T distribution of Fig. 4, where the uncertainty band is particularly narrow for small transverse momenta. Whether this additional jet veto gives rise to a sufficiently stable theoretical approximation in the sense of an experimentally applicable strategy, does highly dependent on the phenomenological question we ask, i.e. the phase-space region we are interested in. Additional jet radiation, as can already be inferred from figure 3, is kinematically unsuppressed to large extent, especially when considering hard events with large transverse momenta. Vetoing additional radiation in a region of phase-space where it becomes likely is crucial to the flat scale

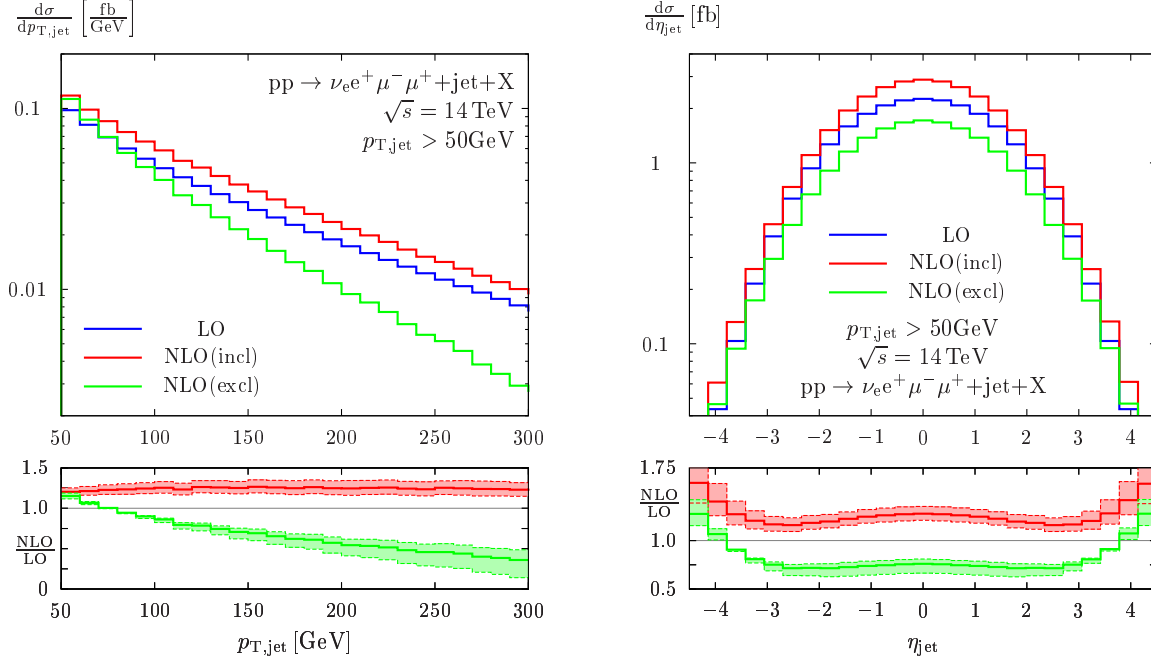


Figure 4: LO, NLO-inclusive and NLO-exclusive differential distributions of the transverse momentum of the hardest jet and its pseudorapidity for W^+Z +jet production including leptonic decays. The differential K -factor band corresponds to varying $\mu_R = \mu_F$ by a factor two around the central scale in the NLO distribution only.

dependence of the exclusive cross section. We discuss this in more detail in Sec. 3.4.

3.4 Differential distributions at the LHC

We now turn to the effect of QCD corrections to the full processes $pp \rightarrow 3 \text{ leptons} + \cancel{E}_T + \text{jet} + X$. Including the leptonic decays with the selection criteria quoted in section 3.1 yields the cross sections given in table 1 at $\mu_R = \mu_F = M_W$ for the inclusive and the vetoed sample, respectively. In table 1 we additionally give a precision comparison of the cross sections calculated with our two programs described in Sec. 2.

The differences of W^-Z +jet compared to W^+Z +jet production are predominantly due to the different parton distribution functions of the incoming partons in the dominating subprocesses. In particular, there are no initial-state up-quarks involved in W^-Z +jet at LO, but in W^+Z +jet.

	Program 1	Program 2
$\sigma_{\text{incl, decay}}^{\text{NLO}}(W^-Z + \text{jet})$	7.4592 [48] fb	7.4628 [63] fb
$\sigma_{\text{incl, decay}}^{\text{NLO}}(W^+Z + \text{jet})$	11.129 [10] fb	11.1286 [47] fb
$\sigma_{\text{excl, decay}}^{\text{NLO}}(W^-Z + \text{jet})$	4.6721 [62] fb	4.6663 [64] fb
$\sigma_{\text{excl, decay}}^{\text{NLO}}(W^+Z + \text{jet})$	6.6900 [92] fb	6.6816 [49] fb

Table 1: Comparison of the numerical results from both of our programs to verify their excellent statistical agreement on the per-mill level for $pp \rightarrow 3 \text{ leptons} + \cancel{E}_T + \text{jet} + X$.

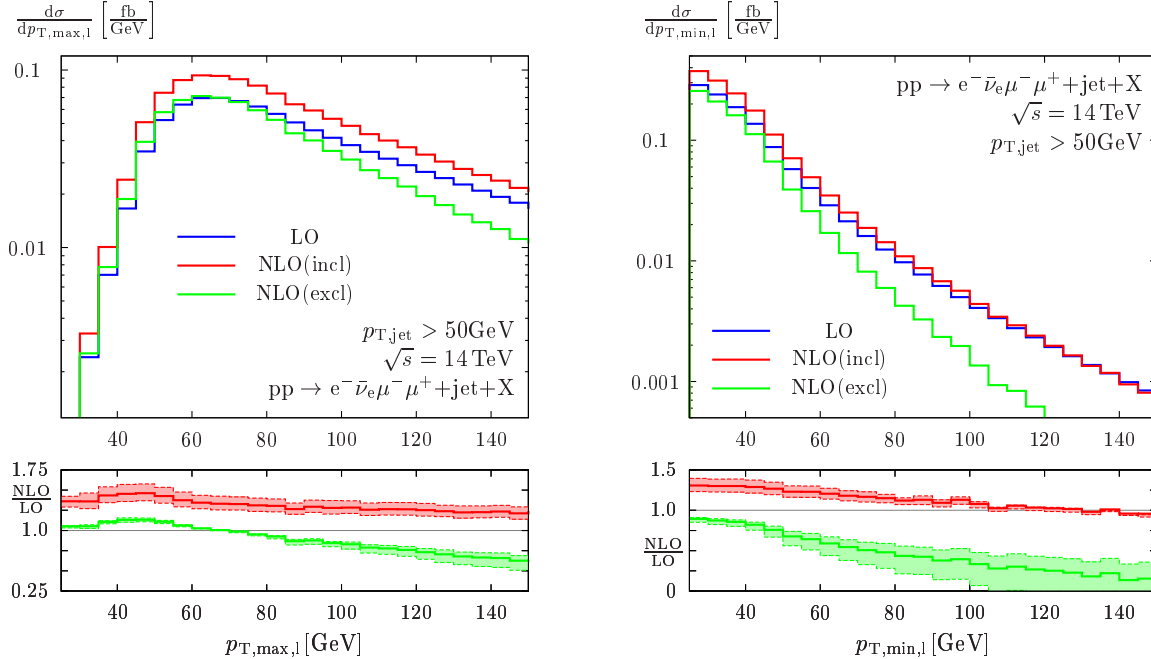


Figure 5: LO, NLO-inclusive and NLO-exclusive differential distributions of the maximum and minimum lepton transverse momentum for W^-Z +jet production. The differential K -factor band corresponds to varying $\mu_R = \mu_F$ by a factor two around the central scale in the NLO distribution only.

From figures 4–7 we uncover a substantial observable-specific phase-space dependence of the QCD corrections. While additional jet radiation gives sizable contributions to the maximum- $p_{T,jet}$ distribution at large values, the LO approximation considerably overestimates the NLO-exclusive findings. Additionally, for inclusive events, the jets tend to be more central due to the extra hard jet emission, which occurs central at small rapidity differences with respect to the other reconstructed jet.

The harder inclusive jets balance against a softer inclusive lepton- p_T spectrum, figure 5, and additional QCD radiation. Apart from this significant deviation of the leptonic distributions from the total $\sigma^{\text{NLO}}/\sigma^{\text{LO}}$ -rescaling, the bulk of the leptonic observables receive only minor differential distortions compared to rescaled-LO when including inclusive-NLO precision. Representatively, we show the maximum and minimum charged-lepton pseudo-rapidity in figure 6 and the tri-lepton invariant mass

$$m_{\text{leptons}}^2 = (p_{e^-} + p_{\mu^+} + p_{\mu^-})^2 \quad (3.15)$$

and the transverse WZ cluster mass in figure 7. The transverse cluster mass

$$m_{\text{T,cluster}}^2 = \left(\sqrt{m^2(e^- \mu^+ \mu^-) + \vec{p}_T^2(e^- \mu^+ \mu^-) + |\not{p}_T|^2} \right)^2 - (\vec{p}_T(e^- \mu^+ \mu^-) + \not{p}_T)^2, \quad (3.16)$$

is a convenient observable to observe production of additional charged heavy bosons [10,33] from a beyond-the-SM sector via Jacobian peaks.

The exclusive distributions, even though improved perturbative stability is suggested from the decreased scale dependence of the total cross sections, which can be observed in

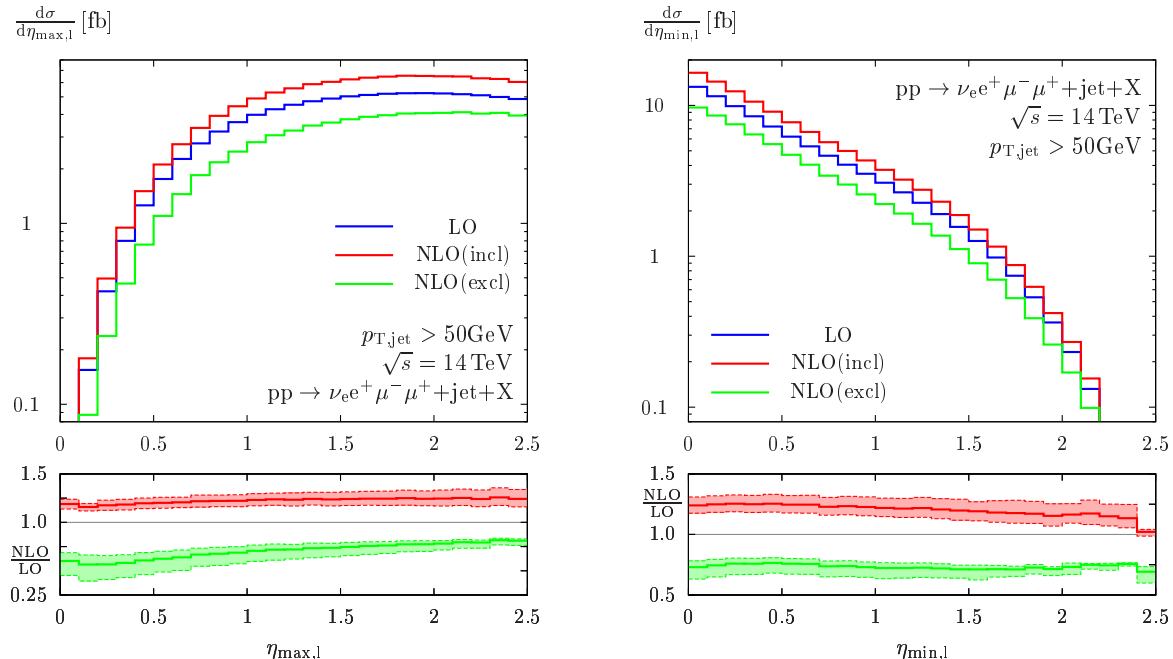


Figure 6: LO, NLO-inclusive and NLO-exclusive differential distributions of the maximum and minimum lepton’s pseudorapidity for W^+Z +jet production. The differential K -factor band corresponds to varying $\mu_R = \mu_F$ by a factor two around the central scale in the NLO distribution only.

figure 3, exhibit large uncertainties, especially in the tails of the p_T distributions. Here additional jet radiation becomes probable as can be seen from the maximum jet- p_T distribution in figure 4. The improved NLO stability of the exclusive sample shows up as perturbative improvement almost exclusively around the threshold region. For the phase-space regions characterized by larger values of p_T , applying the additional jet veto does not yield a stable result anymore—at least in the chosen setup. As shown in figure 5, perturbative control over the exclusive production cross section is already lost at scales of about 100 GeV while the inclusive differential cross section turns out to be reasonably stable. Obviously the jet-veto with a fixed p_T threshold, although hinting at appealing properties by the exclusive cross sections’ flat scale variations, does not easily give rise to a more reliable cross section prediction within the given order of perturbation theory.

4. Summary

We have computed NLO QCD cross sections and differential distributions for $W^\pm Z$ production in association with a hadronic jet at hadron colliders. The calculation has been extended to full leptonic final states at the LHC, where they are well-observable. We find the total QCD corrections to be sizeable at both the Tevatron and the LHC. At the same time they show strong phase-space dependencies in hadronic, semi-hadronic, and especially in transverse momentum distributions. Hence, QCD modifications should be taken into account in every phenomenological study that employs these processes.

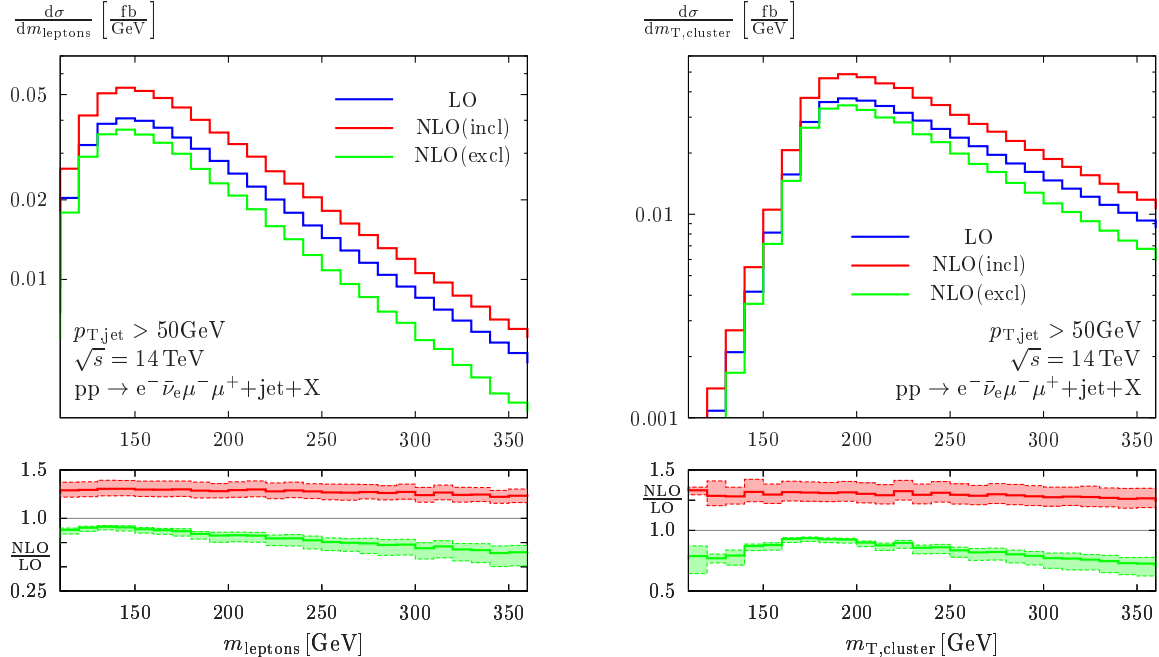


Figure 7: LO, NLO-inclusive and NLO-exclusive differential distributions of the tri-lepton invariant mass m_{leptons} and the transverse cluster mass for $W^-Z+\text{jet}$ production. The differential K -factor band corresponds to varying $\mu_R = \mu_F$ by a factor two around the central scale in the NLO distribution only.

In addition, we demonstrate that the superficial perturbative improvement for exclusive production at the LHC, which is also observed in the various other massive di-boson+jet production cross sections [1–5], does not give rise to perturbatively stable predictions once the additional-jet veto’s impact on the large p_T region is taken into account. The exclusive production’s reduced scale variation therefore expresses NLO stability for a part of our calculation which actually is given to NLO precision. This discrimination between NLO QCD one-jet and LO di-jet contributions, which is inherent to fixed-order calculations, can not be carried over to experimental strategies in a straightforward way, and, hence, does not easily give rise to a phenomenologically applicable method.

Acknowledgments

F. C. acknowledges partial support by FEDER and Spanish MICINN under grant FPA2008-02878. C. E. is supported by “KCETA Strukturiertes Promotionkolleg” and would like to thank the Institute for Theoretical Sciences at the University of Oregon for its hospitality during the time when this work was completed. S. K. would like to thank Stefan Dittmaier for a number of helpful discussions particularly in the initial stage of this work. This research is partly funded by the Deutsche Forschungsgemeinschaft under SFB TR-9 “Computergestützte Theoretische Teilchenphysik”, and the Helmholtz alliance “Physics at the Terascale”, and by the EU’s Marie-Curie Research Training Network HEPTOOLS under contract MRTN-CT-2006-035505.

References

- [1] J. M. Campbell, R. Keith Ellis and G. Zanderighi, *JHEP* **0712** (2007) 056
- [2] S. Dittmaier, S. Kallweit and P. Uwer, *Phys. Rev. Lett.* **100**, 062003 (2008)
- [3] S. Dittmaier, S. Kallweit and P. Uwer, *Nucl. Phys. B* **826**, 18 (2010)
- [4] F. Campanario, C. Englert, M. Spannowsky and D. Zeppenfeld, *Europhys. Lett.* **88**, 11001 (2009)
- [5] T. Binoth, T. Gleisberg, S. Karg, N. Kauer and G. Sanguinetti, *Phys. Lett. B* **683** (2010) 154
- [6] H. Murayama, I. Watanabe and K. Hagiwara, KEK-Report 91-11, 1992
- [7] J. Alwall *et al.*, *JHEP* **0709** (2007) 028
- [8] K. Arnold *et al.*, *Comput. Phys. Commun.* **180** (2009) 1661
- [9] G. Bozzi, B. Jager, C. Oleari and D. Zeppenfeld, *Phys. Rev. D* **75** (2007) 073004, C. Englert, B. Jager and D. Zeppenfeld, *JHEP* **0903** (2009) 060,
- [10] C. Englert, B. Jager, M. Worek and D. Zeppenfeld, *Phys. Rev. D* **80** (2009) 035027, C. Englert, B. Jager, M. Worek and D. Zeppenfeld, arXiv:0904.2119 [hep-ph].
- [11] T. Gleisberg, S. Hoche, F. Krauss, M. Schonherr, S. Schumann, F. Siegert and J. Winter, *JHEP* **0902** (2009) 007
- [12] R. Mertig, M. Bohm and A. Denner, *Comput. Phys. Commun.* **64** (1991) 345
- [13] T. Hahn, *Comput. Phys. Commun.* **140** (2001) 418
- [14] G. Passarino and M. J. G. Veltman, *Nucl. Phys. B* **160**, 151 (1979)
- [15] A. Denner and S. Dittmaier, *Nucl. Phys. B* **658** (2003) 175, *Nucl. Phys. B* **734** (2006) 62
- [16] R. K. Ellis and G. Zanderighi, *JHEP* **0802** (2008) 002
- [17] K. Hagiwara and D. Zeppenfeld, *Nucl. Phys. B* **313** (1989) 560
- [18] S. Catani and M. H. Seymour, *Nucl. Phys. B* **485** (1997) 291 [Erratum-*ibid.* **B 510** (1998) 503]
- [19] T. Figy, V. Hankele and D. Zeppenfeld, *JHEP* **0802** (2008) 076.
- [20] S. Dittmaier, *Phys. Rev. D* **59** (1999) 016007
- [21] T. Hahn and M. Perez-Victoria, *Comput. Phys. Commun.* **118** (1999) 153
- [22] G. J. van Oldenborgh and J. A. M. Vermaseren, *Z. Phys. C* **46**, 425 (1990)
- [23] G. J. van Oldenborgh, *Comput. Phys. Commun.* **66** (1991)
- [24] S. Dittmaier, *Nucl. Phys. B* **675** (2003) 447
- [25] Z. Bern, L. J. Dixon and D. A. Kosower, *Nucl. Phys. B* **412** (1994) 751
- [26] A. Bredenstein, A. Denner, S. Dittmaier and S. Pozzorini, *JHEP* **0808** (2008) 108
- [27] F. A. Berends, R. Pittau and R. Kleiss, *Nucl. Phys. B* **424** (1994) 308
- [28] R. Kleiss and R. Pittau, *Comput. Phys. Commun.* **83**, 141 (1994)
- [29] A. Denner, S. Dittmaier, M. Roth, and D. Wackerroth, *Nucl. Phys. B* **560** (1999), 33, C. Oleari and D. Zeppenfeld, *Phys. Rev. D* **69** (2004), 093004.

- [30] J. Pumplin, D. R. Stump, J. Huston, H. L. Lai, P. Nadolsky, and W. K. Tung, JHEP **0207** (2002), 012
- [31] S. D. Ellis and D. E. Soper, Phys. Rev. D **48** (1993) 3160
- [32] S. Catani, Y. L. Dokshitzer, M. H. Seymour, and B. R. Webber, Nucl. Phys. B **406** (1993), 187.
- [33] J. Bagger *et al.*, Phys. Rev. D **49** (1994), 1246, J. Bagger *et al.*, Phys. Rev. D **52** (1995), 3878.